Transactions of Tianjin University (2021) 27:147–154
https://doi.org/10.1007/s12209-020-00278-0

RESEARCH ARTICLE

Enhancing Photocatalytic Performance of NH_2-UIO66 by Defective Structural Engineering

Zhenmin Xu[1,2] · Jiazhen Cao[2] · Xiang Chen[2] · Liyi Shi[1] · Zhenfeng Bian[2]

Received: 27 October 2020 / Revised: 8 November 2020 / Accepted: 23 November 2020 / Published online: 1 February 2021

Abstract

NH_2-UIO66 (NU) is a promising photocatalyst for the reduction of Cr(VI) to low-toxic Cr(III) driven by visible light under ambient conditions. However, the main limitation in this process is the inefficient ligand to metal charge transfer (LMCT) of photo-excited electrons, which is caused by inherent energy gap (ΔE_{LMCT}). This study synthesized the defective NU (NUX-H, where X is the molar equivalent of the modulator) with reduced ΔE_{LMCT} through linkers removal via acid treatment. The electronic structure of NUX-H was systematically investigated, and the results indicated that the structural defects in NUX-H strongly altered the environment of the Zr atoms. Furthermore, they substantially lowered the energy of the unoccupied d orbitals (LUMO), which was beneficial to efficient LMCT, resulting in an improved photocatalytic activity of NUX-H toward high-concentration (100 mg/L) Cr(VI) reduction. Compared to NU with defect-free structure, the reducing rate of Cr(VI) was increased by 47 times. This work introduced an alternative strategy in terms of designing efficient photocatalysts for reducing Cr(VI) under ambient conditions.

Keywords NH_2-UIO66 · Defective structure · Efficient LMCT · Photocatalysis · Cr(VI) reduction

Introduction

Due to the negative impacts of such a practice on human health and the ecological environment, the discharge of heavy metals from various industrial processes into water has attracted increasing attention worldwide [1–3]. As one of the most environmentally hazardous heavy metals, the widely used hexavalent chromium [Cr(VI)] can be commonly found in the wastewater originating from various industrial processes, such as electroplating, metal finishing, and leather tanning [4–6]. Cr(VI) is difficult to degrade and easy to accumulate in organisms via the food chain, resulting in gene mutation and the canceration of humans and animals even under slight exposure due to its high carcinogenicity and solubility [7–9]. Various techniques have been adopted to remove Cr(VI) from wastewater, including chemical precipitation [10], electrochemical processing [11], adsorption [12], and membrane filtration [13]. Among these techniques, the photocatalytic reduction of Cr(VI) into low-toxic Cr(III) is one of the most promising technologies because of its energy efficiency, high efficiency, and environmental friendliness [14, 15]. However, most photocatalysts, such as TiO_2 [16], ZnO [17], C_3N_4 [18] and WO_3 [19], exhibit limited abilities to reduce Cr(VI) due to their narrow visible light adsorption, poor Cr(VI) adsorption uptake, and low charge carrier separation efficiency [20]. To achieve high Cr(VI) reduction efficiency under visible light, a strategy of designing and synthesizing of efficient and economical photocatalysts is highly desired.

Metal–organic frameworks (MOFs), which represent an emerging class of versatile porous material, are constructed through the coordination bonds between organic linkers and inorganic metal nodes (metal ions or clusters) [21, 22]. Organic linkers in MOFs can generally serve as antennas, and harvest light could make them behave

Zhenmin Xu and Jiazhen Cao have contributed equally to this work.

✉ Liyi Shi
shiliyi@shu.edu.cn

✉ Zhenfeng Bian
bianzhenfeng@shnu.edu.cn

[1] Research Center of Nano Science and Technology, Shanghai University, Shanghai 200444, China

[2] The Education Ministry Key Laboratory of Resource Chemistry, Shanghai Key Laboratory of Rare Earth Function Materials, Shanghai Normal University, Shanghai 200444, China

as semiconductors via the ligand to metal charge transfer (LMCT) process, thus proving that MOFs can be an interesting platform for a broader range of photocatalytic applications [23–25]. In terms of the photocatalytic process, the inherent energy gap (ΔE_{LMCT}) of pristine MOFs is involved in the usage of energy to induce photo-excited electrons to transfer from the linker to a metal node's unoccupied d orbital (LUMO), and thus serves as the main influencing factor that ensures the efficiency of electronic transfers in the LMCT process [26]. Hence, reduced ΔE_{LMCT} is required to achieve efficient LMCT and enhance photocatalytic activity. Actually, only limited kinds of pristine MOFs have been used to perform photocatalytic Cr(VI) reduction with undesirable activity. This is because high energy is required to overcome the positive potential of ΔE_{LMCT}, which in turn, efficiently transfers photo-excited electrons to the metal nodes from the organic linker.

One of the strategies to decrease ΔE_{LMCT} and facilitate photocatalytic activity is through the use of mixed organic linkers or through the addition of another transition metal. However, the metal atoms/clusters are fully coordinated and insufficiently exposed as active sites, which can compromise the process [27, 28]. Defect engineering by removing a number of linkers is the alternative way to optimize the electronic structure of MOFs and improve the photocatalytic Cr(VI) reduction activity, but remain rarely unexplored [29].

In the current study, NH_2-UIO66 was chosen as a representative type of MOFs due to its remarkable tunability, extraordinary visible light response, and excellent thermal stability. To obtain effective LMCT and enhance photocatalytic activity, defective NH_2-UIO66-X–H (NUX-H) with missing linkers through removing a number of 2-aminoterephthalic acid (HATA) linkers from the pristine NH_2-UIO66 and combining modulated synthesis using benzoic acid (HBC) as the modulator with acid treatment (Fig. 1a). In comparison to the pristine NU, higher surface area and larger pore volume of NUX-H were obtained with more linkers when per Zr node was removed. The loss of ligands led to the unsaturated coordination of Zr metal, which in turn, increased the exposure of the Zr atoms and acted as the active adsorption sites in photocatalytic Cr(VI) reduction. Furthermore, the change in electronic environment of the Zr atoms substantially lowered the energy of the d orbitals, resulting in an efficient LMCT. Therefore, the optimal defective NU12-H exhibited outstanding stability and activity in Cr(VI) reduction. This was characterized by the synergistic effects of adsorption and photocatalysis under visible light, by which the Cr(VI) reduction efficiency was about 47 times higher than that of pristine NU.

Experimental

Preparation of Defective NH_2-UIO66-X-H

$ZrCl_4$ (1.0 mmol), 2-aminoterephthalic acid (HATA, 1.0 mmol), and different equivalents of benzoic acid HBC (6, 12, 18, and 24 mmol) were dissolved in DMF (60 mL). This mixture was transferred to a 100 mL Teflon-lined stainless steel autoclave and heated in an oven at 110 °C for 24 h. The obtained solids were purified by DMF and ethanol and then dried. The resulting solids were acid treated with 1 mol/L HCl for 30 min, after which they were centrifuged, washed with water, and then dried under vacuum at 110 °C to obtain defective NH_2-UIO66-X-H powders. These were denoted as NUX-H.

Photocatalytic Reduction of Cr(VI)

In brief, 50 mg catalyst was added to a home-made reactor with 50 mL mixture chromium solution (100 mg/L $Cr_2O_7^{2-}$, pH ~ 3 controlled by HCl). After reaching the adsorption–desorption equilibrium, the photocatalytic reaction was initiated by a Xe light with a 420 nm cut-off filter. The Cr(VI) concentration was analyzed at given time intervals by a UV spectrophotometer (UV 7502/PC) at the characteristic wavelength, from which the reduction yield was calculated.

Characterization

The crystal structure of the as-made samples was studied by X-ray diffraction (XRD, D/MAX-2000 with Cu Kα radiation), and the morphology analysis was performed by field emission scanning electron microscopy (FESEM, HITACHI S4800). The UV–Vis diffuse reflectance spectra (DRS) were measured by a UV–Vis spectrophotometer (UV–Vis DRS, Shimadzu UV-2450). The Barrett–Joyner–Halenda (BJH) model was used to calculate pore volume (V_p) and pore diameter (d_p), and the Brunauer–Emmett–Teller (BET) method was used to calculate the specific surface area (SBET). X-ray photoelectron spectroscopy (XPS, PHI 5000 Versaprobe II) was employed to determine the surface electronic states. The Fourier transform infrared spectra (FT-IR) were obtained on an AVATAR 370 FT-IR spectrometer. The solid state C NMR analysis was conducted using Bruker AVANCEIII 400 MHz. The photoelectrochemical measurements were carried out in a conventional three-electrode, single-compartment quartz cell on an electrochemical station (CHI 660D). A bias voltage of 0.5 V was used to drive the transfer of photogenerated electrons from the working electrode to the platinum electrode. A Na_2SO_4 aqueous

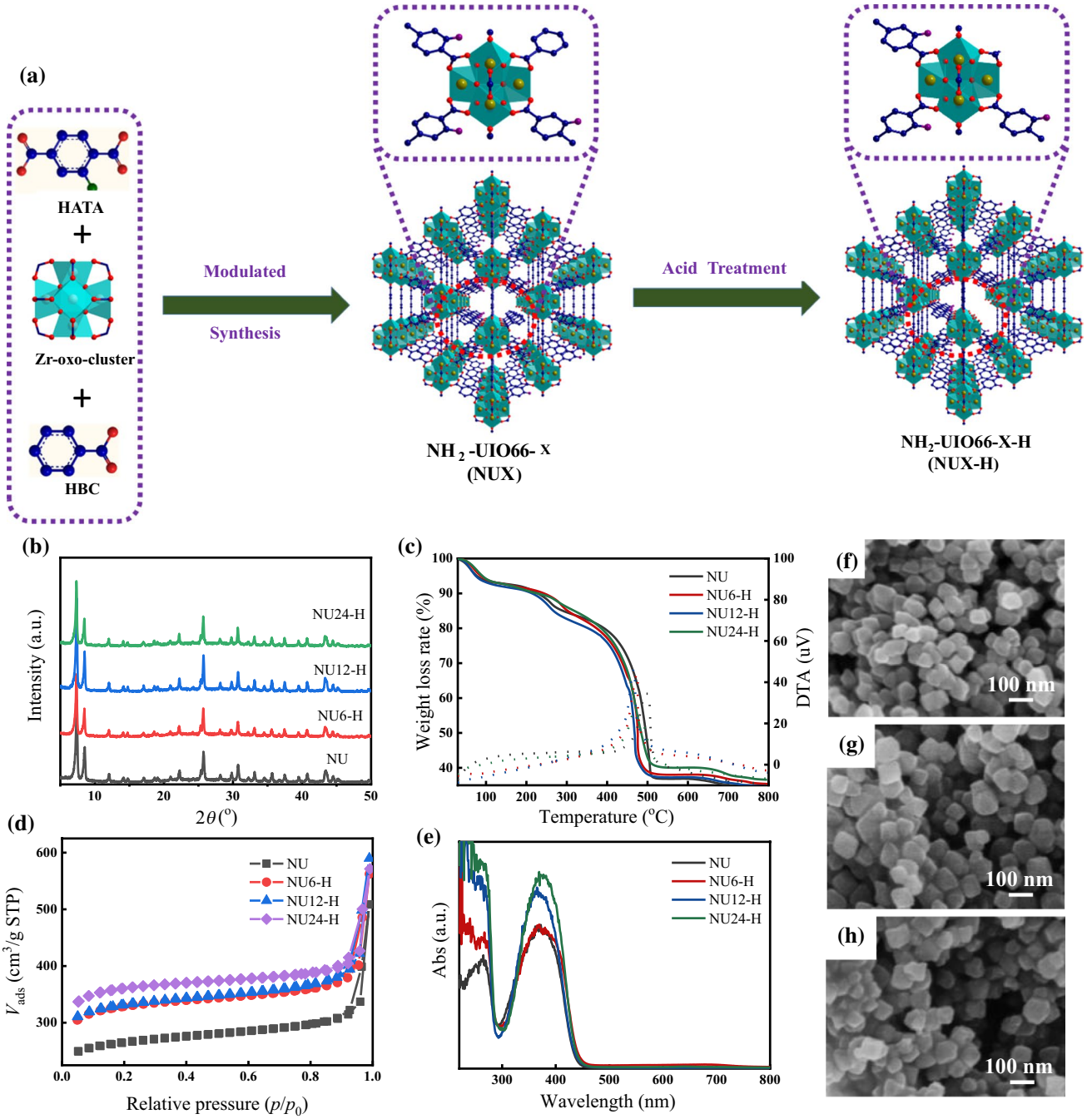

Fig. 1 **a** Schematic illustration of the synthesis of defective NH_2-UIO-66-H (NUX-H). **b** XRD patterns. **c** TGA (solid) plots and DTA (dashed) curves. **d** N_2 adsorption–desorption isotherms and **e** UV–Vis DRS of NU and NUX-H. SEM images of **f** NU, **g** NU12-H, and **h** NU24-H

solution (0.50 mol/L) was used as the electrolyte. A 300 W Xe lamp with a UV filter ($\lambda > 420$ nm) was used as the visible light source; this was positioned 10 cm away from the photoelectrochemical cell. Electrochemical Impedance Spectroscopy (EIS) tests were carried out at the bias voltage of 0.3 V and recorded over a frequency range of $0.01–1 \times 10^5$ Hz with the amplitude of 5 mV.

Results and Discussion

The crystal structures of both defective NUX-H and pristine NU were studied by XRD, as shown in Fig. 1b. No obvious adding peaks were observed, and all NUX-H showed similar XRD patterns with NU, thus indicating that their crystallinity well-remained after the linkers were

removed by acid treatment. The scanning electron microscopy (SEM) image (Fig. 1f–h) showed that NUX-H possessed regularly octahedral crystal with an average length of 100 nm, confirming that the crystal structure is maintained even after acid treatment.

Thermogravimetric analysis (TGA) was adopted to investigate the degree of structural defects in NUX-H (Fig. 1c). All NUX-H samples exhibited two remarkable weight loss steps with the same tendency as that of NU. The weight loss within 30–320 °C can be mainly attributed to the evaporation of DMF and H_2O, both of which were adsorbed in NU. The second weight loss step at the range of 400–500 °C corresponded to the loss of HATA with the collapse of the NU as well as the residual Zr metal nodes as the form of ZrO_2 in the frameworks. The rate of weight loss gradually decreased with the increasing value X, indicating that the incremental defects were created in NUX-H with the removal of more coordinated HBC during the acid treatment.

To further demonstrate the successful removal of HBC in NUX, the amounts of HBC in NU12 before and after acid treatment by C NMR spectra (Fig. S1). Results revealed that, compared with NU12, the peaks corresponding to HBC were absent in NU12-H, suggesting that the HBC serving as the modulator in NUX can be completely removed by acid treatment. The SBET of the NUX increased from 409 to 712 m^2/g, whereas the pore volume did not change significantly (Fig. S2a). Upon the removal of HBC, the SBET of NUX-H further increased to 1106 m^2/g, and the pore volume increased from 0.49 to 0.72 cm^3/g (Fig. 1d, Table 1), suggesting that the missing links in the pore space led to high SBET and increased defects in the NU [30]. Furthermore, the presence of defects had a significant influence on the light absorption capability of NU. As shown in Fig. S2b and Fig. 1e, all NUX exhibited inferior visible light response due to the limited visible absorption of HBC (Fig. S3), which served as the shielding of visible light, thus reducing visible light transmission. Two absorption bands at around 280 and 380 nm, respectively, with enhanced intensity were observed in NUX upon the removal of HBC. These indicated the slight improvement in the light harvesting ability of NUX-H due to the larger pore volume and the elimination of the shield effect.

In order to estimate the influence of defects on photocatalytic performance of NUX-H, the photocatalytic reduction Cr(VI) experiments were conducted in aqueous solution with the initial concentration of 100 mg/L under visible light irradiation. The adsorption abilities of Cr(VI) in different samples were first studied before the photocatalytic experiments (Fig. 2a). As expected, all the defective NUX-H showed higher adsorption capacities than NU, with the adsorption efficiency gradually improving with the increased defect amount. Compared with NUX-H, all NUX with high surface areas showed poor adsorption activities (Fig. S4). This finding indicated that the high-adsorption property of NUX-H was not only related to their surface area, but also attributed to the formation of bared Zr nodes in the HBC removal process, which in turn, acted as the adsorption sites, thus enhancing Cr(VI) adsorption in an acidic solution. On the contrary, there was a negligible change in the Cr(VI) concentration for NU, indicating that NU had slight adsorption behavior due to the smaller surface area and the lack of adsorption sites. The Cr(VI) adsorption ability of photocatalysts plays a vital role in their photoreduction. Therefore, the outstanding adsorption capacity of NUX-H demonstrates its potential use in photocatalytic Cr(VI) reduction.

Our previous studies demonstrated that the Cr(VI) reduction rate could be enhanced in acid solution due to the low reduction potential energy of Cr(VI)/Cr(Ⅲ) [31–34]. Thus, the photocatalytic performance test of Cr(VI) reduction over NUX-H was conducted at pH = 3. This was evaluated by monitoring the UV–Vis spectra toward the Cr(VI) characteristic absorption peak at 350 nm after achieving the adsorption equilibrium [35]. Apparently, both NU and NUX exhibited limited photocatalytic performance of Cr(VI) reduction (Fig. S4). In comparison, Cr(VI) removal with higher efficiency was achieved under the same condition with the HBC removed by acid treatment, indicating that the introduction of defects could enhance the photocatalytic activity of NUX-H. In particular, the photocatalytic activity of NUX-H improved first and then slightly decreased with the increase in the amount of defects, thus presenting a volcano-type trend with increasing structural defects. A similar phenomenon was also observed in photocatalytic H_2 production by Ma [36], in which the defective NH_2-UIO66 modulated by HOAc was used. The result suggested that the amount of defects served as an important factor affecting the photocatalytic performance of NUX-H. Furthermore, an appropriate amount of defect proved to be critical in achieving optimal photocatalytic Cr(VI) removal efficiency.

The linear kinetic curves of Cr(VI) reduction were fitted according to the quasi second-order dynamic equation. As shown in Fig. 2d, the NU12-H exhibited the highest Cr(VI) reduction rate, and the rate constant was calculated to be 0.83961 min^{-1}, which corresponded to 47 times higher than that of pristine NU (Fig. 2e). These suggest that the photoexcited electrons of NU12-H could transfer more easily from linker (HATA) to Zr nodes than those of pristine NU, thus resulting in enhanced activity.

The optimal photocatalyst NU12-H was further applied to reduce Cr(VI) with different Cr(VI) concentrations at a pH value of 3. The results (Fig. 2c) showed that almost 100%

Table 1 Structural parameters of different samples

Item	NU	NU6-H	NU12-H	NU24-H
S_{BET} (m^2/g)	490	980	1090	1106
V_p (cm^3/g)	0.49	0.59	0.64	0.72

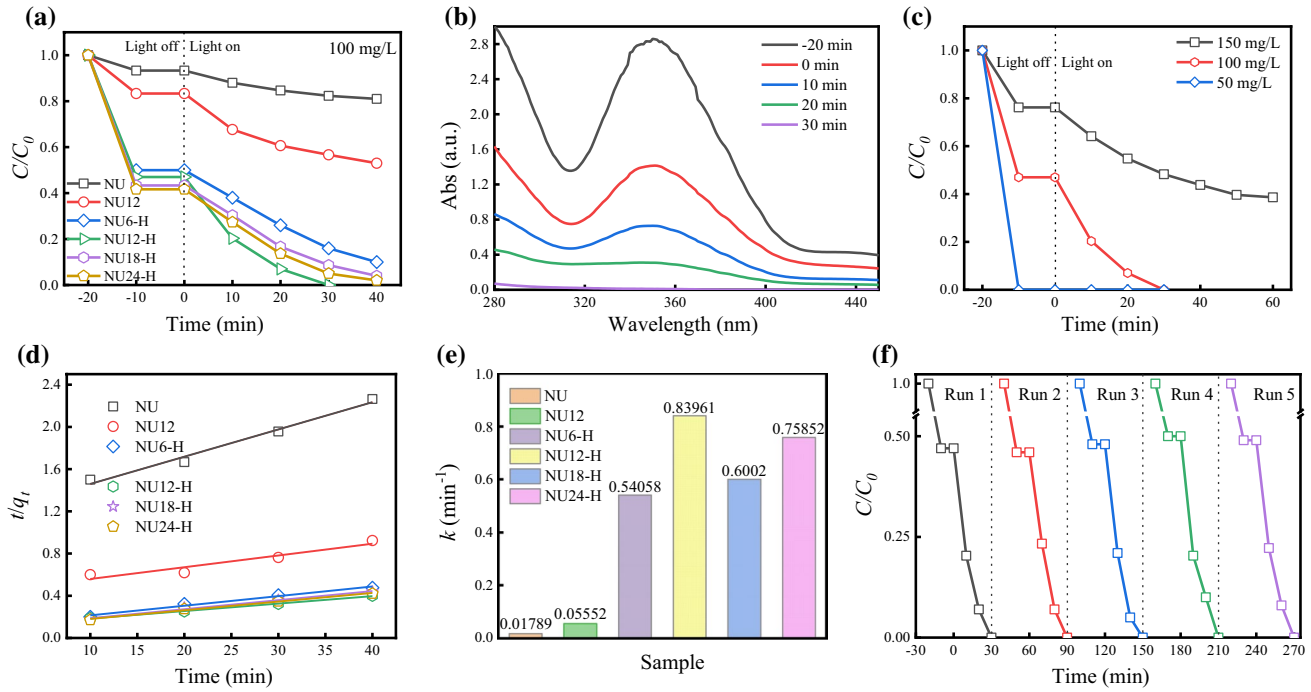

Fig. 2 **a** Photocatalytic Cr(VI) removal activity over different samples. **b** UV adsorption curves of Cr(VI) over NU12-H at different times. **c** Photocatalytic activity of NU12-H toward various Cr(VI) concentrations. **d** Dynamic curves of Cr(VI) removal. **e** Rate constant of photocatalytic reduction Cr(VI) over different samples. **f** Reusability of NU12-H for the photocatalytic reduction of Cr(VI)

Cr(VI) was removed within 10 min due to the excellent adsorption capacity of NU12-H when the concentration of Cr(VI) was 50 mg/L. More importantly, NU12-H still displayed high photocatalytic Cr(VI) reduction efficiency even when Cr(VI) concentration was as high as 150 mg/L. The photocatalytic stability of NU12-H was investigated by successively working without special treatment, except washing and drying after each worked. As described in Fig. 2f, the higher removal efficiency of Cr(VI) was maintained after repeating five times; no obvious decay of catalytic activity and light absorption was observed, and the structure was also preserved (Fig. S5), suggesting that NU12-H possessed excellent recyclability. The above results suggested that NU12-H had good photocatalytic activity and outstanding stability, indicating their positive application prospects in the treatment of industrial wastewater with high concentration of Cr(VI).

In this study, Mott–Schottky plots were employed to further study the band structure of NU at the frequency of 1000 Hz, with the aim of deeply understanding the photocatalytic mechanism of defective MOFs. As shown in Fig. 3a, both NU and NU12-H exhibited positive slopes according to the characteristic of n-type semiconductors [37, 38]. The values of the flat band potential of both NU and NU12-H based on the curves of the Mott–Schottky plots were estimated to be − 0.45 V and − 0.5 V, respectively, versus those of Ag/AgCl, which corresponded to − 0.41 V and − 0.46 V versus NHE, respectively. The LUMO of NU12-H was more negative than that of NU, indicating that the missing linkers altered the environment of the Zr atoms (as determined by FT-IR in Fig. S6) and substantially lowered the energy of the unoccupied d orbitals (LUMO). These are consistent with the findings of Arthur using time-dependent density-functional theory calculations [39]. Importantly, the negative LUMO can strongly decrease the ΔE_{LMCT}, thus facilitating an efficient LMCT process. Furthermore, the photogenerated electrons more easily migrated to the adsorbed Cr(VI), which was proved to be more favorable for Cr(VI) photoreduction.

Photocurrent and EIS measurements were also conducted to investigate the charge transfer and separation behaviors of defective NUX-H. As shown in Fig. 3b,c, defective NUX-H exhibited higher photocurrent density and smaller arc radius than those of NU under the same conditions. Moreover, the Photoluminescence (PL) spectral intensities of defective NUX-H were lower than those of NU (Fig. 3d), implying that the defective structure reduced the ΔE_{LMCT} and led to efficient LMCT. In turn, this resulted in higher separation efficiency and lowered recombination rate. Among all defective NUX-H, NU12-H presented the highest charge separation efficiency. This indicates that the optimal level of defective structure is critical to the efficient transfer of photo-excited charge.

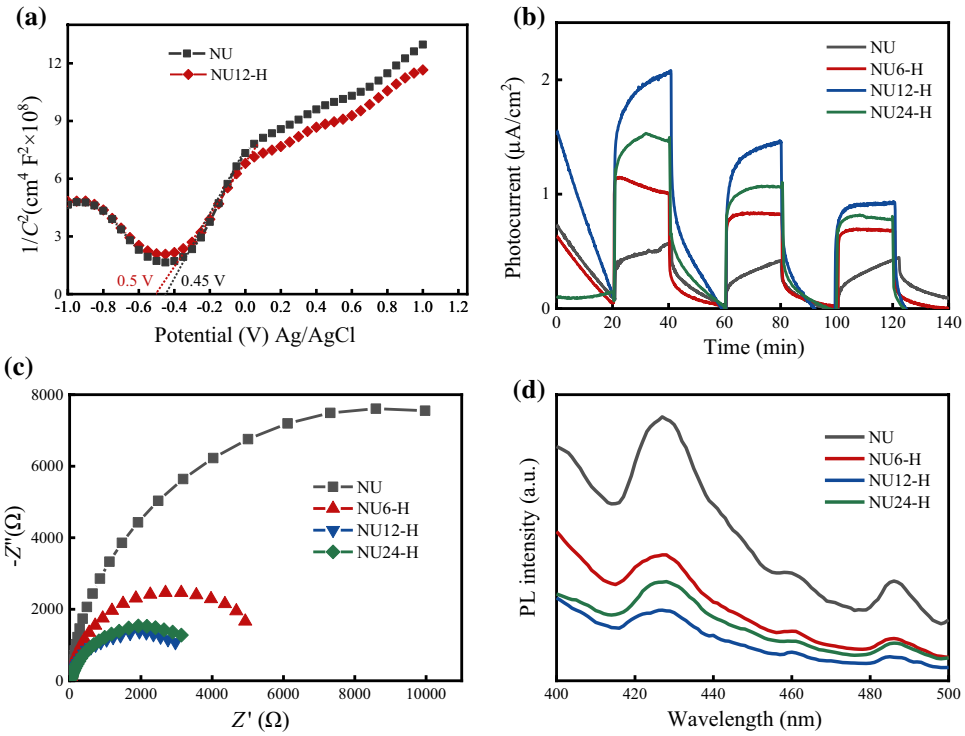

Fig. 3 **a** Mott–Schottky plots, **b** Transient photocurrent response, **c** EIS Nyquist plots, and **d** PL curves of different samples

Conclusion

In this work, an efficient photocatalyst with outstanding stability, the defective NH_2-UIO66 (NUX-H) with missing linkers was synthesized via post-synthetic acid treatment. The defective structures were verified by N_2 adsorption–desorption isotherm, TGA, and solid state C NMR. The results showed that defective NUX-H possessed both higher SBET and larger pore volume than NU with a defect-free structure. In addition, NUX-H with the optimized level of defects exhibited the highest photocatalytic activity in high-concentration Cr(VI) reduction. Due to the efficient LMCT caused by the creation of defects, the reduction rate as high as 0.83961 min^{-1} was 47 times higher than that of NU.

Moreover, the mechanism of the significant enhanced efficiency of charge transfer was systematically investigated via Mott–Schottky plots, transient photocurrent response, and EIS Nyquist plots. The results showed that the introduction of defects by missing linkers can lead to an efficient LMCT process due to the reduced ΔE_{LMCT}, which improved the photocatalytic performance of Cr(VI) reduction. This work introduced an alternative strategy to designing efficient photocatalysts, which is expected to offer a sustainable application in both Cr(VI) reduction and Cr(III) removal from the aqueous phase when combined with adsorption, photo-electrocatalysis, and membrane separation.

Supplementary information The online version of this article (https://doi.org/10.1007/s12209-020-00278-0) contains supplementary material, which is available to authorized users.

Acknowledgements This work was supported by the National Key Research and Development Program of China (No. 2020YFA0211000), the National Natural Science Foundation of China (Nos. 21876114, 21761142011, and 51572174), the Shanghai Government (Nos. 19DZ1205102 and 19160712900), the International Joint Laboratory on Resource Chemistry (No. IJLRC), and the Ministry of Education of China (No. PCSIRT_IRT_16R49). This research was also supported by The Program for Professor of Special Appointment (Eastern Scholar) at Shanghai Institutions of Higher Learning, the Shuguang Research Program of Shanghai Education Committee, and the Shanghai Engineering Research Center of Green Energy Chemical Engineering (No. 18DZ2254200).

References

1. Xie XQ, Chen C, Zhang N et al (2019) Microstructure and surface control of MXene films for water purification. Nat Sustain 2(9):856–862
2. El-Sheikh SM, Azzam AB, Geioushy RA et al (2020) Visible-light-driven 3D hierarchical Bi_2S_3/BiOBr hybrid structure for superior photocatalytic Cr(VI) reduction. J Alloys Compd 857(15):157513
3. Li QH, Dong M, Li R et al (2021) Enhancement of Cr(VI) removal efficiency via adsorption/photocatalysis synergy using electrospun chitosan/g-C_3N_4/TiO_2 nanofibers. Carbohydr Polym 253:117200
4. Liu SX (2005) Removal of copper (VI) from aqueous solution by Ag/TiO_2 photocatalysis. Bull Environ Contam Toxicol 74(4):706–714
5. Ravishankar TN, Vaz MO, Ramakrishnappa T et al (2017) Ionic liquid assisted hydrothermal syntheses of Au doped TiO_2 NPs for efficient visible-light photocatalytic hydrogen production from water, electrochemical detection and photochemical detoxification of hexavalent chromium (Cr^{6+}). RSC Adv 7(68):43233–43244
6. Tanaka A, Nakanishi K, Hamada R et al (2013) Simultaneous and stoichiometric water oxidation and Cr(VI) reduction in aqueous suspensions of functionalized plasmonic photocatalyst Au/TiO_2-Pt under irradiation of green light. ACS Catal 3(8):1886–1891
7. Gowda UC, Reddy NL, Shankar MV et al (2020) One-pot synthesis of Cu–TiO_2/CuO nanocomposite: application to photocatalysis for enhanced H_2 production, dye degradation & detoxification of Cr(VI). Int J Hydrog Energy 45:7813–7828
8. Zhou L, Wang LZ, Lei JY et al (2017) Fabrication of TiO_2/Co-g-C_3N_4 heterojunction catalyst and its photocatalytic performance. Catal Commun 89:125–128
9. Luo DY, Yan RH, Fu CY et al (2019) Cu(0)/TiO_2 composite byproduct from photo-reduction of acidic Cu-containing wastewater and its reuse as a catalyst. J Water Process Eng 32:100958
10. Yao FB, Jia MC, Yang Q et al (2020) Electrochemical Cr(VI) removal from aqueous media using titanium as anode: simultaneous indirect electrochemical reduction of Cr(VI) and in-situ precipitation of Cr(III). Chemosphere 260:127537–127547
11. Zuo KC, Huang XC, Liu XC et al (2020) A hybrid metal–organic framework-reduced graphene oxide nanomaterial for selective removal of chromate from water in an electrochemical process. Environ Sci Technol 54:13322–13332
12. Mehmet EA, Sukru D, Celalettin O et al (2007) Heavy metal adsorption by modified oak sawdust: thermodynamics and kinetics. J Hazard Mater 141:77–85
13. Lu MM, Gao F, Li C et al (2020) Response of microalgae chlorella vulgaris to cr stress and continuous cr removal in a membrane photobioreactor. Chemosphere 262:128422–128431
14. Mei QF, Zhang FY, Wang N et al (2019) TiO2/Fe2O3 heterostructures with enhanced photocatalytic reduction of Cr(vi) under visible light irradiation. RSC Adv 9(39):22764–22771
15. Xu ZM, Zheng R, Chen Y et al (2019) Ordered mesoporous Fe/TiO_2 with light enhanced photo-Fenton activity. Chin J Catal 40(5):631–637
16. Kanakaraju D, Shahdad NRBM, Lim YC et al (2019) Concurrent removal of Cr (III), Cu (II), and Pb(II) ions from water by multifunctional TiO_2/Alg/FeNPs beads. Sustain Chem Pharm 14:100176
17. Abbas KK, Al-Ghaban AMHA (2019) Enhanced solar light photoreduction of innovative TiO_2 nanospherical shell by reduced graphene oxide for removal silver ions from aqueous media. J Environ Chem Eng 7(3):103168
18. Yang XB, Qiu LQ, Luo XT (2018) ZIF-8 derived Ag-doped ZnO photocatalyst with enhanced photocatalytic activity. RSC Adv 8(9):4890–4894
19. Bai LQ, Huang HW, Zhang SG et al (2020) Photocatalysis-assisted Co_3O_4/g-C_3N_4 p–n junction all-solid-state supercapacitors: a bridge between energy storage and photocatalysis. Adv Sci 7(22):2001939
20. Li YY, Wang CH, Zheng H et al (2017) Surface oxygen vacancies on WO_3 contributed to enhanced photothermo-synergistic effect. Appl Surf Sci 391:654–661
21. Wang XS, Chen CH, Ichihara F et al (2019) Integration of adsorption and photosensitivity capabilities into a cationic multivariate metal–organic framework for enhanced visible-light photoreduction reaction. Appl Catal B Environ 253:323–330
22. Wang CC, Du XD, Li J et al (2016) Photocatalytic Cr(VI) reduction in metal–organic frameworks: a mini-review. Appl Catal B Environ 193:198–216
23. Li R, Zhang W, Zhou K (2018) Metal–organic-framework-based catalysts for photoreduction of CO_2. Adv Mater 30(35):1705512
24. Long JL, Wang SB, Ding ZX et al (2012) Amine-functionalized zirconium metal–organic framework as efficient visible-light photocatalyst for aerobic organic transformations. Chem Commun 48(95):11656
25. Shen LJ, Liang SJ, Wu WM et al (2013) Multifunctional NH_2-mediated zirconium metal–organic framework as an efficient visible-light-driven photocatalyst for selective oxidation of alcohols and reduction of aqueous Cr(vi). Dalton Trans 42(37):13649
26. Nasalevich MA, Hendon CH, Santaclara JG et al (2016) Electronic origins of photocatalytic activity in d (0) metal organic frameworks. Sci Rep 6:23676
27. Melillo A, Cabrero-Antonino M, Navalón S et al (2020) Enhancing visible-light photocatalytic activity for overall water splitting in UiO-66 by controlling metal node composition. Appl Catal B Environ 278:119345
28. Syzgantseva MA, Ireland CP, Ebrahim FM et al (2019) Metal substitution as the method of modifying electronic structure of metal–organic frameworks. J Am Chem Soc 141:6271–6278
29. Shearer GC, Chavan S, Ethiraj J et al (2014) Tuned to perfection: ironing out the defects in metal–organic framework UiO-66. Chem Mater 26(14):4068–4071
30. Wang KK, Li CF, Liang YX et al (2016) Rational construction of defects in a metal–organic framework for highly efficient adsorption and separation of dyes. Chem Eng J 289:486–493
31. Xu ZM, Deng XM, Chen Y et al (2020) Engineering a rapid charge transfer pathway for enhanced photocatalytic removal efficiency of hexavalent chromium over C_3N_4/NH_2-UIO-66 compounds. Sol RRL 5: 202000416
32. Zhang YX, Xu MJ, Li H et al (2018) The enhanced photoreduction of Cr (VI) to Cr (III) using carbon dots coupled TiO_2 mesocrystals. Appl Catal B Environ 226:213–219
33. Ling LL, Liu LF, Feng YW et al (2018) Synthesis of TiO_2 mesocrystal film with enhanced photocatalytic activity. Chin J Catal 39(4):639–645
34. Deng XM, Chen Y, Wen JY et al (2020) Polyaniline-TiO_2 composite photocatalysts for light-driven hexavalent chromium ions reduction. Sci Bull 65(2):105–112
35. Li YL, Bian YY, Qin HX et al (2017) Photocatalytic reduction behavior of hexavalent chromium on hydroxyl modified titanium dioxide. Appl Catal B Environ 206:293–299
36. Ma X, Wang L, Zhang Q et al (2019) Switching on the photocatalysis of metal–organic frameworks by engineering structural defects. Angew Chem Int Edit 58(35):12175–12179

37. Zhang X, Dong H, Sun XJ et al (2018) Step-by-step improving photocatalytic hydrogen evolution activity of NH_2-UiO-66 by constructing heterojunction and encapsulating carbon nanodots. ACS Sustain Chem Eng 6(9):11563–11569
38. Wang YN, Guo LN, Zeng YQ et al (2019) Amino-assisted NH_2-UiO-66 anchored on porous g-C_3N_4 for enhanced visible-light-driven CO_2 reduction. ACS Appl Mater Inter 11(34):30673–30681
39. Arthur DV, Hendrickx K, Pascal VDV et al (2017) Missing linkers: an alternative pathway to UiO-66 electronic structure engineering. Chem Mater 29(7):3006–3019

Liyi Shi is a professor in the Research Center of Nano Science and Technology at Shanghai University. His main research area is the development and application of novel nanomaterials with tunable size and controllable structure. He is also devoted to the industrialization of nanotechnology.

Zhenfeng Bian received his Ph.D. degree in Environmental Chemistry from Shanghai Normal University in 2010. He has been a JSPS postdoctoral fellow in the laboratory of professor Tetsuro Majima during 2010–2013. He joined Shanghai Normal University in 2013 as a full professor, and acquired the National Science Fund for Excellent Young Scholars in 2015. His research interests are focused on the design and synthesis of TiO2-based nanomaterials for environmental and energy photocatalysis.